Supporting Information

Study on a TCM Evaluation Method Based on MIP Modified MOFs Sensor with Highly Selective Electrocatalytic Activity — An *Artemisia Annua L.* Perspective

Jingbo Zhang[a, †], Quancheng Chen[a, †], Xuemin Gao[a], Ziqin Suo[a], Di Wu[a], Yunxian Zhou[a], Yingying Zeng[a], Yanping Li[c], Yanyun Che[b,*], Qing Chen[a,*]

[a]*Fujian Provincial Key Laboratory of Innovative Drug Target Research, School of Pharmaceutical Sciences, Xiamen University, Xiamen 361102, PR China.*
[b]*China Engineering Research Center for Homology of medicine and food beverage of Yunnan Province,Yunnan University of Chinese Medicine, Kunming 650500, PR China.*
[c]*Department of Pharmacy, the First affiliated hospital of Xiamen university, School of Medicine,Xiamen University, Xiamen 361000 PR China.*
[†]*These authors contributed equally to this work.*
**Corresponding author.*

E-mail addresses: chenqing@xmu.edu.cn (Qing Chen); checpu@163.com (Yanyun Che)

Author contributions
Jingbo Zhang, Quancheng Chen: Conceptualization, Methodology, Validation, Formal analysis, Data Curation, Writing – Original and Visualization. Xuemin Gao, Ziqin Suo and Di Wu: Conceptualization, Methodology, Investigation and Writing – Review & Editing. Yunxian Zhou, Yingying Zeng and Yanping Li: Methodology and Validation. Yanyun Che: Resources, Supervision and Funding acquisition. Qing Chen: Resources, Supervision, Project administration and Funding acquisition.

Reagents and apparatus

Short carboxylated multi-walled carbon nanotubes (MWCNT, 95%),α-methacrylic acid (MAA, 99%), 5,10,15,20-tetrakis-(4-carboxyphenyl)-porphyrin-Fe-(III) chloride (FeTCPPCl, AR), Dibenzoyl peroxide (BPO, 99%), N, N-diethylformamide (DEF, 99%), N, N-dimethylformamide (DMF, 99.5%), Heptane (HA, 98%), chitosan (bioreagent), Dihydroartemisinin (DHA, 98%), Artesunate (ASE, 99%) and phosphate buffer solution (PBS 10× pH = 7.4) were purchased from Macklin (Shanghai, China). $ZrOCl_2 \cdot 8H_2O$ (99.5%) was purchased from Sinopharm Chemical Reagent (Shanghai, China). Potassium ferricyanide (99.5%), potassium ferrocyanide (99.5%), benzoic acid (99.5%), anhydrous alcohol (99.5%), anhydrous Acetic acid (99.5%) and potassium chloride (AR) were purchased from Xilong Scientific (Shantou, China). Artemisinin (ART, 98%) and Ethylene Glycol Dimethacrylate (EGDMA, 98%) was purchased from Aladdin Biochemical Technology (Shanghai, China). N, N-bis(2-hydroxypropyl)-p-toluidine (DPOPT, 95%) and potassium bromide (spectro) was purchased from Acmec Biochemical (Shanghai, China). Acetonitrile (HPLC) was purchase from Thermo Scientific (U.S.). Ultrapure water was purified via Milli-Q® Advantage.

Electrochemical measurements were performed with a CHI660E and CHI1030C electrochemical workstation (CH Instruments, Shanghai, China). The morphology and elemental composition of samples were examined using Zeiss SUPRA55 scanning electron microscope (SEM). Fourier transform infrared spectroscopy (FTIR) was conducted using a Thermo Scientific Nicolet iS10 spectrometer. X-ray diffraction analysis (XRD) was performed on a Shimadzu XRD-7000 X-Ray Diffractometer. Particle size measurement was performed on a Malven Nano-ZS90 dynamic laser scattering (DLS) Zetasizer.

Note S1. Material preparation

1. Preparation of MOF-525(Fe)

Three hundred mg of $ZrOCl_2 \cdot 8H_2O$ (0.93 mmol), 100 mg of FeTCPPCl (0.12 mmol), and 3.3 g of benzoic acid (27 mmol) were dissolved in 100 mL of DEF. After ultrasonic dispersion for 10 minutes, the resulting uniform solution was transferred to a 250 mL blue-cap bottle. The blue-cap bottle containing the solution was then placed in an oven. Once the oven temperature reached 90°C, it was maintained for 5 hours, and the dark brown precipitate was collected by centrifugation. Subsequently, the obtained product was washed with DMF, centrifuged at 8000 rpm for 10 minutes, and repeated three times until the washing solution was colorless. It was then washed with methanol, centrifuged at 8000 rpm for 10 minutes, and repeated six times to remove residual DMF. Finally, the product was placed in a vacuum drying oven and dried overnight at 60°C to obtain the final product, MOF-525(Fe).

2. Preparation of MOF-525(Fe)@MWCNT

Three hundred mg of $ZrOCl_2 \cdot 8H_2O$ (0.93 mmol), 100 mg of FeTCPPCl (0.12 mmol), and 3.3 g of benzoic acid (27 mmol) were dissolved in 100 mL of DEF. After adding 150 mg of MWCNT, the mixture was ultrasonically dispersed for 10 minutes. The resulting uniform solution was then transferred to a 250 mL blue-cap bottle.

The blue-cap bottle containing the solution was placed in an oven. Once the oven temperature reached 90°C, it was maintained for 5 hours, and the dark brown precipitate was collected by centrifugation. The subsequent washing and drying steps were the same as those described for MOF-525(Fe).

Note S2. Experiments

1. DLS size measurement

To obtain the particle size distribution of the MOF-525(Fe)@MWCNT-MIP sample, 1 mg of the sample was dispersed in 10 mL of methanol. The mixture was then ultrasonicated for 1 hour to achieve a stable dispersion. After that, 2 mL of the dispersion was transferred to a polystyrene Malvern particle size sample cell. The sample cell was placed in the particle size analyzer for testing, resulting in the particle size distribution of the sample.

2. SEM test

To observe the surface morphology of the MOF-525(Fe)@MWCNT-MIP sample, 1 mg of the sample was dispersed in 10 mL of methanol and ultrasonicated for 1 hour to obtain a stable dispersion. Then, 10 μL of the dispersion was pipetted and dropped onto a silicon wafer. After the liquid naturally air-dried, the silicon wafer was mounted onto the SEM sample holder using conductive carbon tape. The sample was placed into the electron microscope chamber and observed using the SE2 detector of the microscope at an accelerating voltage of 3.0 kV and a magnification of 30 K times.

3. FT-IR test

Take approximately 5 mg of the sample and about 200 mg of spectroscopically pure potassium bromide. Place them in an agate mortar and grind them uniformly. After grinding, take an appropriate amount of the mixture and add it to the pelletizing mold until the bottom of the sample trough is fully covered. After pelletizing, place the sample in a Fourier transform infrared spectrometer for testing.

Based electro-chemical reaction

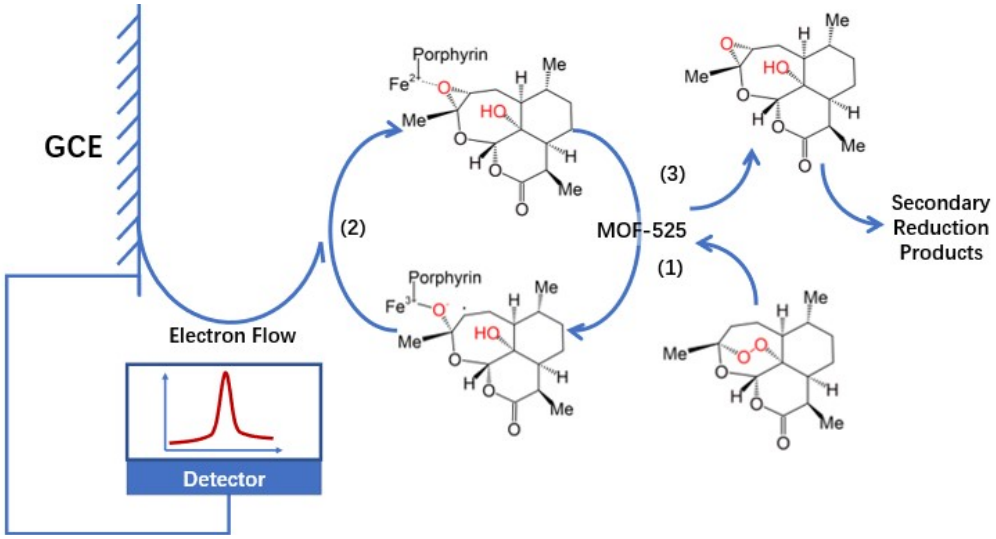

Figure S1 - Electro-reduction of ART on MOF-525(Fe) modified GCE.

During this process, ART interacts with the electrode surface-modified MOF-525(Fe) and undergoes an electrochemical reduction reaction under the influence of an applied voltage (as shown in Fig. S1). The current signal generated by this reaction process is directly proportional to the concentration of ART in the system. Therefore, by monitoring changes in the current signal at a specific reaction potential, the concentration of ART can be accurately converted into a measurable current signal, enabling sensitive detection of ART(Chen, 1999). This method not only demonstrates the potential application of iron porphyrin ligand-containing MOFs in the field of electrochemical sensors but also provides an effective and highly selective new approach for the detection of ART and similar compounds with

endoperoxides structures.

Optimization and screening of synthesis and detection conditions

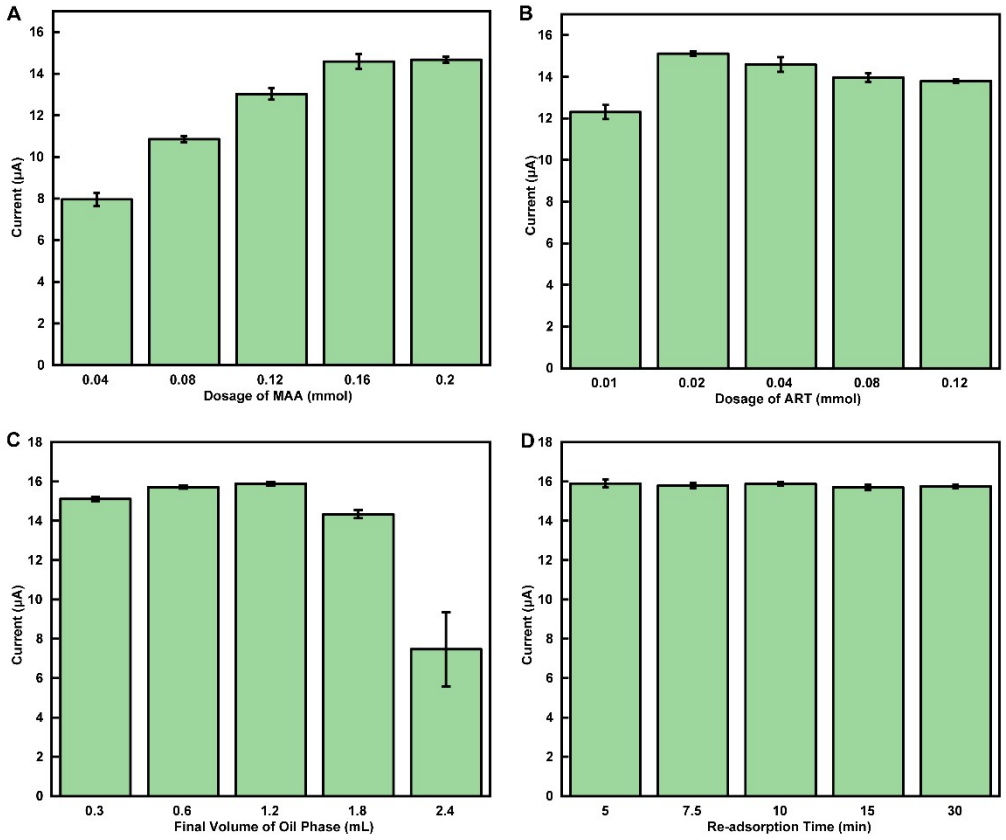

Figure S2 - Current response of serial MOF-525(Fe)@MWCNT-MIP modified GCE prepared under different conditions and measured after serial time of re-adsorption. A) Current response of MOF-525(Fe)@MWCNT-MIP prepared with MAA dosage of 0.04, 0.08, 0.12, 0.16, 0.20 mmol; B) Current response of MOF-525(Fe)@MWCNT-MIP prepared with ART dosage of 0.01, 0.02, 0.04, 0.08, 0.12 mmol; C) Current response of MOF-525(Fe)@MWCNT-MIP prepared with final volume of oil phase of 0.3, 0.6, 1.2, 1.8, 2.4 mmol; D) Current response of MOF-

525(Fe)@MWCNT-MIP modified GCE after the time of 5, 7.5, 10, 15, 30 min for re-adsorption..

The synthesis conditions for MOF-525(Fe)@MWCNT-MIP were screened and optimized based on Table S1. Seventeen sets of synthesized materials (excluding samples 1, 2, 4, and 5 used for particle size comparison) were tested and their current response peaks at -0.5 V in a 0.01 M ART solution were recorded. The results are shown in Figure S2.

According to Figure S2(A), the current response value of the material increases with the increasing amount of functional monomer MAA and does not significantly increase after 0.16 mmol. This indicates that before this amount, the adsorption capacity of the microspheres for ART increases with the increasing amount of MAA. Regarding the amount of template molecule ART, as shown in Figure S2(B), the response signal of the material reaches its maximum when using a feed amount of 0.02 mmol and then slowly decreases with increasing feed amount. This may be due to the formation of fewer effective imprinting sites at lower template molecule concentrations, while at higher concentrations, there is competitive binding between the template molecules and functional monomers, which also prevents the formation of sufficient imprinting sites. Figure S2(C) reflects the

effect of the amount of porogen on the adsorption efficiency of imprinted microspheres. It can be observed that before the oil phase volume reaches 1.2 mL, the response current increases with increasing amounts of porogen HA. However, after 1.2 mL, the response current decreases with increasing HA usage. We considered it was owing to that when the amount of porogen is small, the material porosity was low, resulting in weaker adsorption capacity, however, too high an amount of porogen could enable some analytes to pass through the material and reach the electrode surface for reaction without undergoing the corresponding electrocatalytic process, thus also leading to a decrease in characteristic peak current. Finally, according to Figure S2(D), it can be found that there is no significant difference in the response current when the material's re-adsorption time is set to 5, 7.5, 10, 15, or 30 minutes. This indicates that the material has already reached adsorption equilibrium before 5 minutes.

The optimal preparation conditions for MIP microspheres and the testing re-adsorption time have been obtained. The conclusion can be drawn that the best microsphere synthesis formula is to use 1.2 mL of deionized water containing 5 mg/mL of MOF-525(Fe)@MWCNT as the aqueous phase and a solution containing 0.16 mmol of MAA, 0.8 mmol of EGDMA, 0.02 mmol of ART, and adjusted to 1.2 mL with HA as the oil phase. It is also concluded that the optimal re-adsorption

time before actual sample testing is only 5 minutes, which can be synchronized with the deoxygenation operation performed before testing, greatly simplifying the operation steps.

Table S1 Formulation of a serial materials and related conditions for synthesis in the process of condition screening.

No.	Concentration of MOF@MWCNT (mg/mL)	Dosage of MAA (mmol)	Dosage of EGDMA (mmol)	Dosage of ART (mmol)	Volume of oil phase（mL）	Volume of water volume (mL)	Re-adsorption time (min)
1	1	0.16	0.8	0.04	0.3	1	10
2	2	0.16	0.8	0.04	0.3	1	10
3	5	0.16	0.8	0.04	0.3	1	10
4	10	0.16	0.8	0.04	0.3	1	10
5	12	0.16	0.8	0.04	0.3	1	10
6	5	0.04	0.8	0.04	0.3	1	10
7	5	0.08	0.8	0.04	0.3	1	10
8	5	0.12	0.8	0.04	0.3	1	10
9	5	0.20	0.8	0.04	0.3	1	10
10	5	0.16	0.8	0.01	0.3	1	10
11	5	0.16	0.8	0.02	0.3	1	10
12	5	0.16	0.8	0.08	0.3	1	10
13	5	0.16	0.8	0.12	0.3	1	10
14	5	0.16	0.8	0.02	0.6	2	10
15	5	0.16	0.8	0.02	1.2	4	10
16	5	0.16	0.8	0.02	1.8	6	10
17	5	0.16	0.8	0.02	2.4	8	10

Table S1 (continued)

No.	Concentration of MOF@MWCNT (mg/mL)	Dosage of MAA (mmol)	Dosage of EGDMA (mmol)	Dosage of ART (mmol)	Volume of oil phase（mL）	Volume of water volume (mL)	Re-adsorption time (min)
18	5	0.16	0.8	0.02	1.2	4	5
19	5	0.16	0.8	0.02	1.2	4	7.5
20	5	0.16	0.8	0.02	1.2	4	15
21	5	0.16	0.8	0.02	1.2	4	30

Characterization of prepared materials

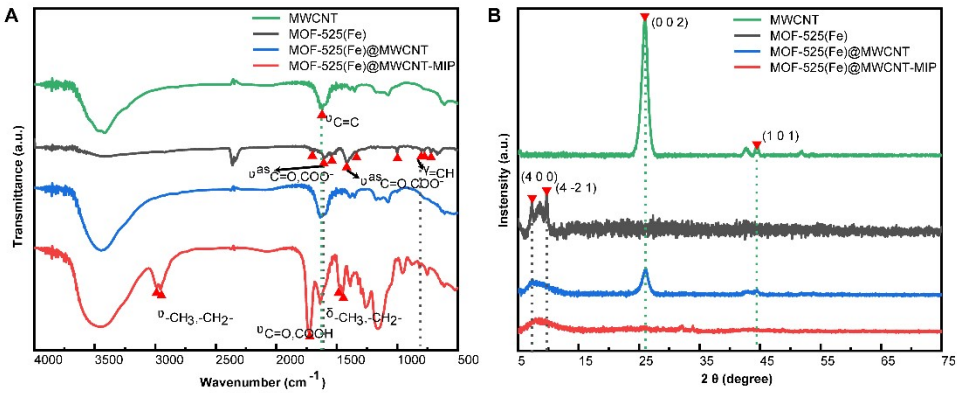

Figure S3 - Characterization of prepared materials. A) FT-IR spectrum of MWCNT, MOF-525(Fe), MOF-525(Fe)@MWCNT, MOF-525(Fe)@MWCNT-MIP; B) XRD spectrum of same materials.

As shown in Figure S3, this is the FT-IR spectra and XRD patterns of the synthesized MOF-525(Fe). In Figure S3(A), we can observe the characteristic C=O stretching vibration peaks of carboxylate (1604, 1418 cm^{-1}), the =CH out-of-plane bending vibration peak (801 cm^{-1}) of the para-disubstituted benzene ring, and other relevant absorption peaks (2923, 1700, 1543, 1340, 999, 777, 721 cm^{-1}) in porphyrin compounds in the MOF-525(Fe) spectrum(Feng et al., 2012). The MOF-525(Fe)@MWCNT spectrum simultaneously exhibits the characteristic C=C backbone stretching vibration peak (1630 cm^{-1}) of MWCNT and the characteristic absorption peaks of

MOF-525(Fe) at 1604 and 801 cm^{-1}. Additionally, in the MOF-525(Fe)@MWCNT-MIP spectrum, besides the three characteristic peaks, the characteristic -CH_3 and -CH_2- stretching vibration peaks (2988, 2954 cm^{-1}) of PMAA, the carboxyl C=O stretching vibration peak (1728 cm^{-1}), and the -CH_3 and -CH_2- bending vibration peaks (1471, 1444 cm^{-1}) can also be observed. The presence of these characteristic peaks demonstrates the successful synthesis of the composite material.

The black curve in Figure S3(B) represents the XRD pattern of MOF-525(Fe). By referencing the literature, two diffraction peaks at 7.1° and 9.9° can be identified, corresponding to the (4 0 0) and (4 -2 1) crystal planes of the material, respectively. The increase in diffraction intensity before 5° is likely due to interlayer diffraction(Safaei Moghaddam et al., 2020), which is common in porphyrin-based MOF materials. The green curve in Figure S3(B) depicts the XRD pattern of MWCNT, where two diffraction peaks at 26.6° and 44.6° corresponding to the (0 0 2) and (1 0 1) crystal planes of MWCNT can be observed(Chen et al., 2014). These four diffraction peaks also appear in the XRD pattern of MOF-525(Fe)@MWCNT (blue curve in Figure S2(B)), further confirming the successful synthesis of the composite material. However, due to the decreased crystallinity of the composite material compared to the

two individual materials, the intensity of each peak has decreased, and the peak shapes have broadened to varying degrees. Moreover, in the spectrum of MOF-525(Fe)@MWCNT-MIP (red curve in Figure S3(B)), the characteristic peaks of MWCNT have become difficult to identify due to the significantly increased dispersion and random spatial orientation of individual MWCNTs. Nonetheless, the characteristic peaks of MOF-525(Fe) remain identifiable due to the higher crystallinity of its grains, thus confirming the successful preparation of the composite material MOF-525(Fe)@MWCNT-MIP.

Test of electrocatalytic ART reduction performance

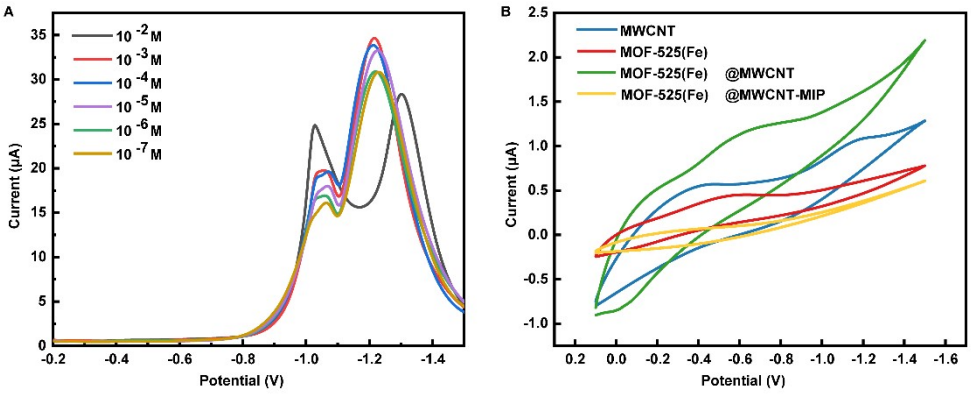

Figure S4 Serial voltammetry curve of different modified electrode in 0.01 M ART solution. A) DPV curve of bare GCE; B) CV curve of GCE modified with MWCNT, MOF-525(Fe), MOF-525(Fe)@MWCNT and MOF-525(Fe)@MWCNT-MIP (with ART re-adsorbed).

As shown in Figure S4, voltametric curves were obtained using different material-modified electrodes in a 0.01 M ART solution. From Figure S4(A), it can be observed that although an unmodified glassy carbon electrode can produce a concentration-dependent reduction peak, its potential is located at a relatively negative value around -1.0 V, and it cannot be completely separated from another unknown reduction peak. This increases the difficulty of subsequent data processing and introduces additional sources of error. Figure S4(B) demonstrates that all three materials used can catalyze the

reduction of ART to varying degrees, thereby reducing its overpotential on the electrode surface. Among them, the MOF-525(Fe)-modified electrode can completely lower the reduction potential of ART to around -0.5 V, but its peak current is relatively low due to its poor conductivity. MWCNTs exhibit a certain degree of catalytic effect, but the peak current at -1.0 V is not eliminated. The composite material of the two achieves both a complete reduction of the potential to around -0.5 V and a higher peak current. Also, after the final step of molecularly imprinting, the peak current drops sharply due to the poor conductivity of MIPs hindering the electron transportation from electrodes to material-solution surface. But the dropped peak can still be recognized at approximately -0.5 V, indicating the same catalyzing activity to MOF-MWCNT hybrid material with the absence of peak at -1.0 V.

Morphological characterization of prepared materials

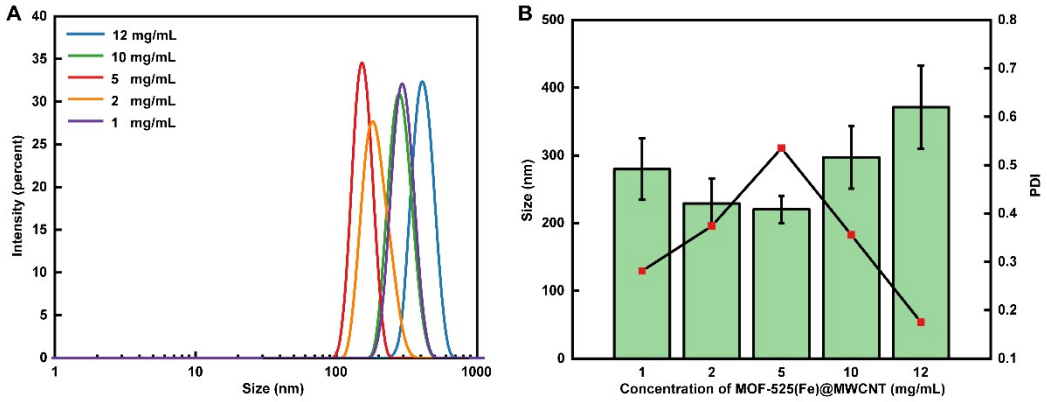

Figure S5 - DLS size measurement of prepared MOF-525(Fe)@MWCNT-MIP with the concentration of MOF-525(Fe)@MWCNT of 1, 2, 5, 10, 12 mg/mL. A) Size intensity distribution; B) Size statistical analysis.

As shown in Figure S5, the particle size distribution (Figure S5(A)) and statistical analysis (Figure S5(B)) of MIP microspheres polymerized in an aqueous phase containing 1, 2, 5, 10 and 12 mg/mL of MOF-525(Fe)@MWCNT are presented. It can be observed that the microspheres obtained using a material concentration of 5 mg/mL have the smallest particle size, implying that the resulting microspheres have the largest specific surface area under these conditions. Relatively speaking, when the amount of emulsifier added is too small, its emulsifying effect on the oil phase is weaker, leading to larger micelle diameters in the emulsion and consequently larger polymer particles. On the other hand, when the amount of emulsifier

added is too large, MOF-525(Fe)@MWCNT itself tends to agglomerate into larger structures, which can also result in larger particle size products.

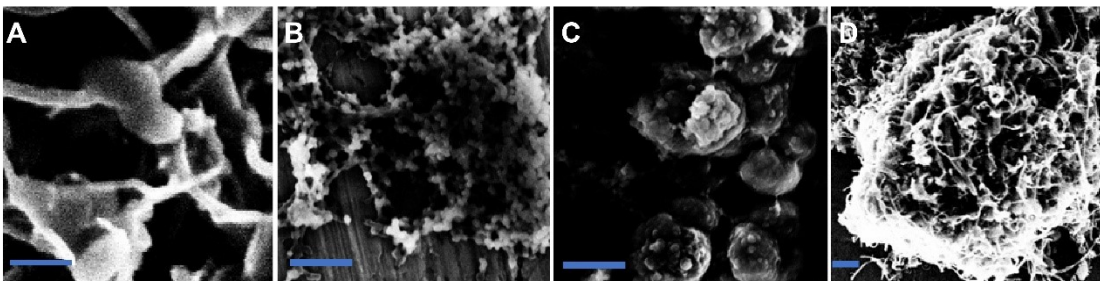

Figure S6 SEM image of prepared materials, scale bar = 200 nm. A) Image of prepared MOF-525(Fe)@MWCNT; B) Image of prepared MOF-525(Fe)@MWCNT-MIP with the concentration of MOF-525(Fe)@MWCNT of 1 mg/mL and C)5 mg/mL, D)12 mg/mL

As shown in Figure S6, SEM images are presented for synthesized MOF-525(Fe)@MWCNT (Figure S6(A)) and MOF-525(Fe)@MWCNT-MIP materials obtained with MOF-525(Fe)@MWCNT concentrations of 1, 5, and 12 mg/mL (Figures S6(B-D), respectively). In Figure S6(A), an intertwined linear structure formed by carbon nanotubes can be observed, with MOF material attached to them. In Figures S6(B) and S6(D), at low concentrations, the product material mainly exhibits a disordered and connected bead-like structure, with no observable potential cavity

structure. At high concentrations, large particulate products are predominantly obtained, and there is a significant amount of exposed MOF-525(Fe)@MWCNT on the surface of the products, which may lead to a decrease in material selectivity. In contrast, the material in Figure S6(C) exhibits a multi-core capsule-like structure that is consistent with literature reports on the preparation of MIP microspheres using similar Pickering emulsion polymerization methods(Wang et al., 2023). Therefore, it is reasonable to choose 5 mg/mL as the optimized concentration of MOF-525(Fe)@MWCNT.

System noise level determination

Table S2 Sensors' current response in blank solution and RSD of signal.

No.	Current response（μA）		No.	Current response（μA）
1	2.333		11	2.319
2	2.329		12	2.319
3	2.341		13	2.321
4	2.328		14	2.330
5	2.306		15	2.324
6	2.344		16	2.328
7	2.311		17	2.328
8	2.322		18	2.325
9	2.318		19	2.322
10	2.320		20	2.323
AVG	2.324	SD	0.008622	RSD 3.72%

As shown in Table S2, the sensor current response values obtained from 20 consecutive parallel measurements in a blank solution without ART. By calculating the standard deviation (SD), the system noise of the sensor is determined to be 8.622×10^{-9} μA, with a relative standard deviation of 3.72%. This also demonstrates the good intermediate precision of the method.

Elution of Template Molecules

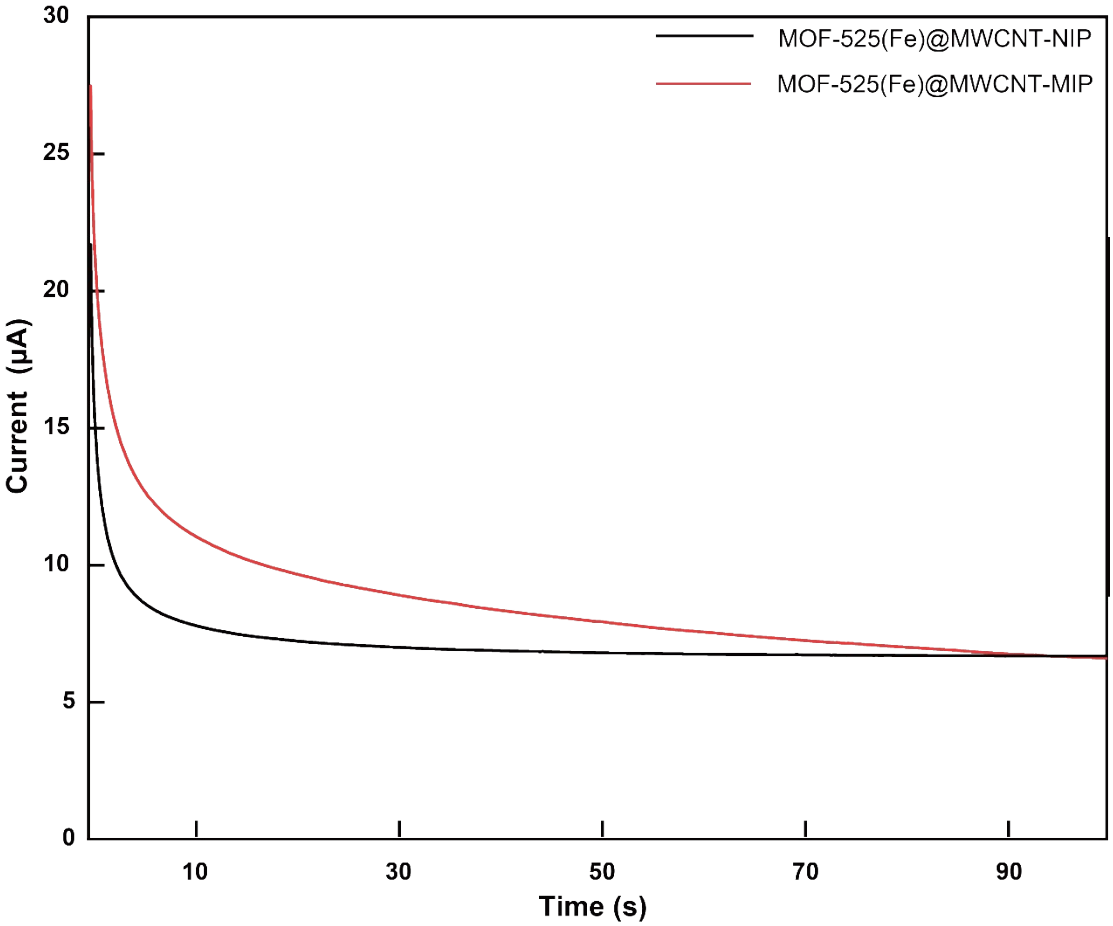

Figure S7 Current changing of MOF-525(Fe)@MWCNT-MIP and MOF-525(Fe)@MWCNT-NIP modified GCE in elution step.

As shown in Figure S7, change in current during the electrostatic elution process for GCEs modified with MOF-525(Fe)@MWCNT-MIP and MOF-525(Fe)@MWCNT-NIP is depicted. It can be observed that the current of the GCE modified with MOF-525(Fe)@MWCNT-NIP quickly reached equilibrium and no longer decreased by 90 seconds, while the current curve for the GCE modified with MOF-525(Fe)@MWCNT-MIP started higher and decreased more slowly. This indicates the continuous reduction of

ART molecules and their detachment from the electrode surface under electrostatic repulsion. After 90 seconds, both curves reached the same equilibrium current, indicating that the ART molecules have been completely eluted. Therefore, setting the elution conditions to -1 V for 100 seconds is reasonable.

DPV curve of MOF-525(Fe)@MWCNT-NIP modified GCE

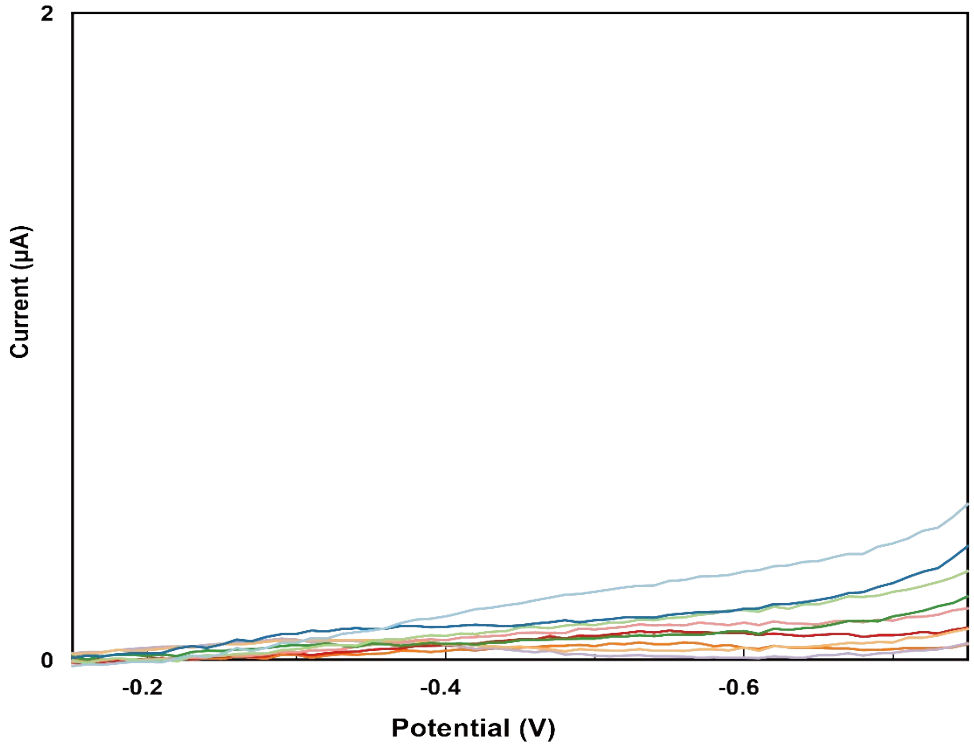

Figure S8 DPV curve of MOF-525(Fe)@MWCNT-MIP modified GCE in 10^{-2} - 10^{-9} M ART solution.

NIP-modified electrode showed a significantly weaker response to ART concentration changes in Figure S8. This implies that, even after elution, the absence of imprinted cavities prevents ART from accessing the catalytic sites, resulting in negligible current variation.

Repeatability of sensors before testing and after testing

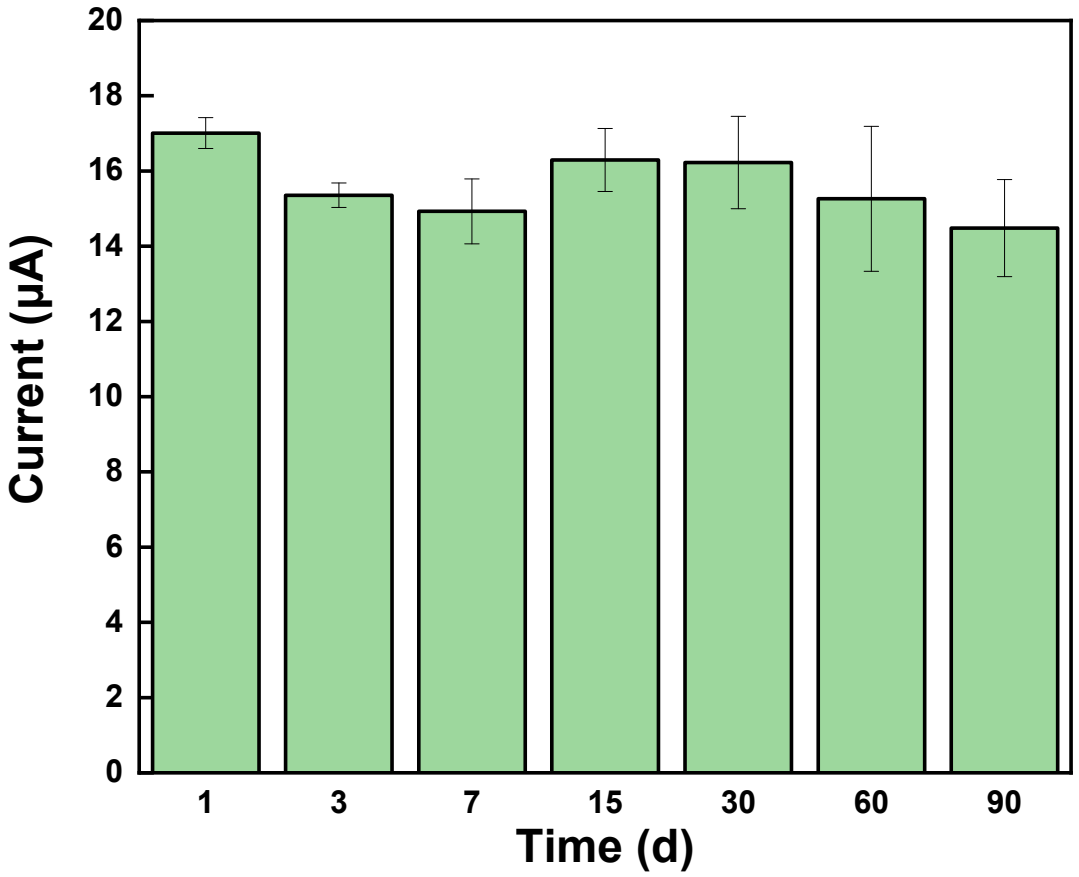

Figure S9. Current response of GCE modified with MOF-525(Fe)@MWCNT-MIP stored for different time in 0.01 M ART solution.

The long-term stability and inter-day reproducibility of the sensor were systematically validated. As shown in Figure S9, the synthesized MOF-525(Fe)@MWCNT-MIP was stored in a sealed container at -20°C in the refrigerator. Portions of the same batch of MOF-525(Fe)@MWCNT-MIP material were taken out on days 1, 3, 7, 15, 30, 60, and 90, respectively, and modified onto GCE. After elutionS

the template ART, the current response values were measured in a 0.01 M ART solution was plotted. The prepared MOF-525(Fe)@MWCNT-MIP exhibited minimal changes in response level over three months. Even at day 60—the point of highest variability—the sensor retained >89.73% of its initial response with an RSD of 12.63%, which remains within acceptable limits for practical applications. By day 90, the sensor still retained >85% of its initial response, with a reduced RSD of 8.91%, demonstrating remarkable stability under prolonged storage (-20°C). These results confirm that the material can be stored for at least three months without performance loss. Furthermore, the consistent response across multiple days (e.g., day 1 to day 90, RSD <12.63%) highlights its robust inter-day reproducibility.

Specific origins and batch numbers of tested *Artemisia annua* samples

Table S3 ART content level obtained from various herbal *Artemisia annua* samples and deteriorated samples (n = 3).

Sample No. & Batch No.	Content level（wt %）	Sample No. & Batch No.	Content level （wt %）
1 AH231001*	0.9890 ± 0.094	9 SD230915	0.2831 ± 0.018
2 AH220628	0.01007 ± 0.00082	10 HB231024	0.7915 ± 0.0072
3 AH231020	0.6184 ± 0.060	11 AH220301	$0.002805 \pm 6.8\times10^{-5}$
4 SC231031	1.2050 ± 0.072	12 DETER1**	$0.001019 \pm 8.3\times10^{-5}$
5 AH220919	0.01028 ± 0.00064	13 DETER3	$0.001037 \pm 6.9\times10^{-5}$
6 AH230615	0.3066 ± 0.026	14 DETER4	$0.001049 \pm 1.7\times10^{-5}$
7 HB220615	0.005193 ± 0.00051	15 DETER6	$0.0009400 \pm 5.4\times10^{-5}$
8 SC220823	0.004895 ± 0.00033	16 DETER10	$0.001077 \pm 3.2\times10^{-5}$

*Batch No. was set with first letters representing origin province (AH: Anhui, SC: Sichuan, HB: Hubei, SD: Shandong), and 6-digit number representing the production date.

** For deteriorated samples, batch No. was set with DETER representing ‘deteriorated’, and the corresponding original sample No.

References

Chen, H., 1999. Decomposition mechanism of an artemisinin-type compound via hemin-electrocatalysis. Talanta 48, 143–150. https://doi.org/10.1016/S0039-9140(98)00230-6

Chen, S., Xin, Y., Zhou, Y., Zhang, F., Ma, Y., Zhou, H., Qi, L., 2014. Branched CNT@SnO_2 nanorods@carbon hierarchical heterostructures for lithium ion batteries with high reversibility and rate capability. J. Mater. Chem. A 2, 15582–15589. https://doi.org/10.1039/C4TA03218G

Feng, D., Gu, Z.-Y., Li, J.-R., Jiang, H.-L., Wei, Z., Zhou, H.-C., 2012. Zirconium-Metalloporphyrin PCN-222: Mesoporous Metal-Organic Frameworks with Ultrahigh Stability as Biomimetic Catalysts. Angew. Chem. Int. Ed. 51, 10307–10310. https://doi.org/10.1002/anie.201204475

Safaei Moghaddam, Z., Kaykhaii, M., Khajeh, M., Oveisi, A.R., 2020. PCN-222 metal–organic framework: a selective and highly efficient sorbent for the extraction of aspartame from gum, juice, and diet soft drink before its spectrophotometric determination. BMC Chemistry 14, 19. https://doi.org/10.1186/s13065-020-00674-6

Wang, Z., Li, Z., Yan, R., Wang, G., Wang, Y., Zhang, X., Zhang, Z., 2023. Facile fabrication of hollow molecularly imprinted

polymer microspheres via pickering emulsion polymerization stabilized with TiO2 nanoparticles. Arabian Journal of Chemistry 16, 105304. https://doi.org/10.1016/j.arabjc.2023.105304